Validation of remote sensing and weather model forecasts in the Agulhas ocean area to 57°S by ship observations

Authors:
Christophe Messager[1]
Vincent Faure[2]

Affiliations:
[1]Laboratoire de Physique des Océans, CNRS, Plouzané Cedex, France

[2]Research Institute for Global Change, Japan Agency for Marine-Earth Science and Technology, Yokosuka, Japan

Correspondence to:
Christophe Messager

Email:
christophe.messager@ifremer.fr

Postal address:
IFREMER/Brest, Laboratoire de Physique des Océans, BP 70, 29280 Plouzané Cedex, France

Dates:
Received: 05 May 2011
Accepted: 12 Oct. 2011
Published: 12 Mar. 2012

How to cite this article:
Messager C, Faure V. Validation of remote sensing and weather model forecasts in the Agulhas ocean area to 57°S by ship observations. S Afr J Sci. 2012;108(3/4), Art. #735, 10 pages. http://dx.doi.org/10.4102/sajs.v108i3/4.735

The region south of South Africa, encompassing the Agulhas Current and Retroflection, and part of the Southern Ocean, is known for its severe meteorological conditions. Because of these conditions, *in-situ* observations are rare. Consequently, remote-sensing satellite observations and high-resolution regional weather forecasts at the ocean surface are difficult to assess. However, atmospheric data collected in the southern hemisphere summer of 2008 during the International Polar Year-BONUS-GoodHope campaign were used to validate two satellite data sets: the twice daily QuikSCAT winds and the daily OAflux data set of latent and sensible heat fluxes. The surface winds and heat fluxes forecasts produced by a regional atmospheric model were also assessed along the ship track. In this study, we have shown that the two data sets exhibited a very good accordance with daily *in-situ* observations. During the campaign, the correlation coefficients for wind speed and direction were 0.97 and 0.91, respectively, and those for latent and sensible heat fluxes were 0.92 and 0.90, respectively. The QuikSCAT wind speed was underestimated by 1.37 m/s relative to *in-situ* data, south of the Subtropical Front. Large differences in heat fluxes in both OAflux and the atmospheric model were observed when crossing the Subtropical Front and a warm eddy, as well as during a storm, when gale force winds reached more than 20 m/s. The two data sets were then used to assess the regional model forecasts over a larger area south of South Africa, not limited to the ship track. Most of the model errors were located in a region north of the Subtropical Front, where the sea surface temperature used by the model was not accurate enough to reproduce the relevant mesoscale oceanic features driving the spatial variability of the surface winds and heat fluxes. Finally, compared to *in-situ* and remote sensing observations, the numerical modelling weather forecast produced realistic atmospheric conditions over the sea south of the Subtropical Front.

Introduction

The Agulhas Current carries warm water along the east coast of South Africa towards the Atlantic Ocean. With an estimated average transport of 69.7 x 10^6 m^3/s off Port Edward (31°S), it is regarded as the strongest western boundary current in the southern hemisphere.[1] South of the tip of Africa, the Agulhas Current changes direction and turns sharply eastward. This tight turn, called the Agulhas Retroflection, produces large eddies propagating westwards in the Atlantic Ocean, contributing to the leakage of large amounts of water from the Indian Ocean to the Atlantic Ocean,[2,3] and regulating the global ocean circulation and climate.[4]

The retroflection also produces numerous smaller eddies and filaments that propagate towards the Southern Ocean. Eddies and filaments carry warm surface waters in areas of cold air and strong westerly winds, producing large heat losses to the atmosphere. These heat losses have a strong impact on the atmosphere boundary layer and influence the ocean–atmosphere coupling.[5,6] In particular, sharp variations of sea surface temperature (SST) associated with eddies and filaments, have been observed to influence wind speed and direction.[7,8,9]

The region of the Agulhas Retroflection is poorly explored despite its strong impact on climate. For this reason, the BONUS-GoodHope cruise took place aboard the French ship R/V *Marion Dufresne* between 16 February and 24 March 2008, as a contribution to the 2008 International Polar Year consensus to gather more observations in the area. The cruise was dedicated to oceanographic sampling, although standard atmospheric measurements were also conducted, allowing for the computation of surface fluxes driving ocean–atmosphere exchanges (including wind, waves and currents).

In addition, an automated operational weather forecast product was developed for the campaign. This dedicated product was needed because standard weather forecasts are often inaccurate as a result of a lack of detailed meteorological data in the area where the cruise took place. High-

resolution 24-h forecasts were received daily at 09:00 UTC on the ship. The forecasts included latent and sensible heat fluxes from the ocean to the atmosphere.

The aim of this work was to assess the weather fields produced by the weather model used for the forecast during the cruise. Firstly, the *in-situ* measurements taken from the ship were used to validate QuikSCAT satellite wind observations, and the OAflux reanalysis product of latent and sensible heat fluxes. Then, the forecasted wind and heat fluxes were compared with *in-situ* data. Finally, the performance of the weather model, relative to satellite and reanalysis data, over a broader region of the Southern Ocean was assessed.

Data and methods

Most of the on-board instruments were installed above the footbridge. However, the wind and temperature data presented here were converted to heights of 10 m and 2 m, respectively. A WEATHERPAK Shipboard Weather Station (Coastal Environmental Systems Inc., Seattle, WA, USA), which included a Young anemometer and temperature and humidity sensors, was deployed. Solar radiation was measured by an Eppleys sensor (Newport, RI, USA). Additionally, an automatic meteorological METEO-FRANCE station 'BATOS' (Toulouse, France) as well as sonic anemometers were installed in the main mast of the ship. A second radiation sensor was installed in the forward ship's mast. Intercomparison and cross validation of all these data were performed in order to obtain the best data set along the ship track. Data corrections included checks for possible instrument failure, superstructure influences, sampling gaps and rain effects. Note that the data for wind intensity and direction are accurate to within ±0.5 m/s and ±5°, respectively, and for relative humidity and air and sea surface temperatures are accurate to within ±2% and 0.1 °C, respectively.

The BONUS-GoodHope ship track consisted of two legs (Figure 1). The first leg was between Cape Town (33.55°S, 18.25°E) and 57°S, 0°E, and had frequent station stops for oceanographic sampling (up to 48 h). The second leg was the ship's return to Durban (30°S, 31°E). The ship track intersected several ocean fronts, starting with the northern Subtropical Front (STF), which defines the Southern Ocean northern limit. The other three fronts found south of the STF – the Subantarctic Front (SAF), Polar Front (PF) and Southern Boundary (SBy) – are part of the Antarctic Circumpolar Current (ACC). Their locations along Leg 1 were determined using the hydrographic data collected during the survey based on classical hydrographic criteria.[11,12] For instance, the SAF is defined by three criteria: a salinity lower than 34.2 practical salinity units (PSU) at a depth of 300 m to the south, a temperature above 4°C – 5°C at a depth of 400 m to the north and an oxygen concentration above 7 mL/L at depths shallower than 200 m to the south.

Figure 2 indicates the positions of the fronts from north to south for Leg 1 (no hydrographic measurements are available along Leg 2). The STF (38.25°S) was crossed on 24 February when the SST abruptly decreased by 5 °C. Note that in the Agulhas Retroflection region, the STF is somewhat discontinuous because of the presence of many eddies[13]; for instance, the strong meridional SST gradient shown in Figure 2e on 24 February was the southern edge of an anticyclonic warm eddy.[14] The SAF (44.17°S) was crossed on 02 March, the PF (50.36°S) was crossed on 08 March, the Southern Antarctic Circumpolar Current Front (SACCF; 53°S) was crossed on 12 March and the SBy (55.73°S) of the Antarctic Circumpolar current was reached on 14 March. The average locations of the fronts (Figure 1) were determined using Argo profiling floats.[10] Argo is a global array of free-drifting profiling floats that measure the temperature and salinity of the upper 2000 m of the ocean.

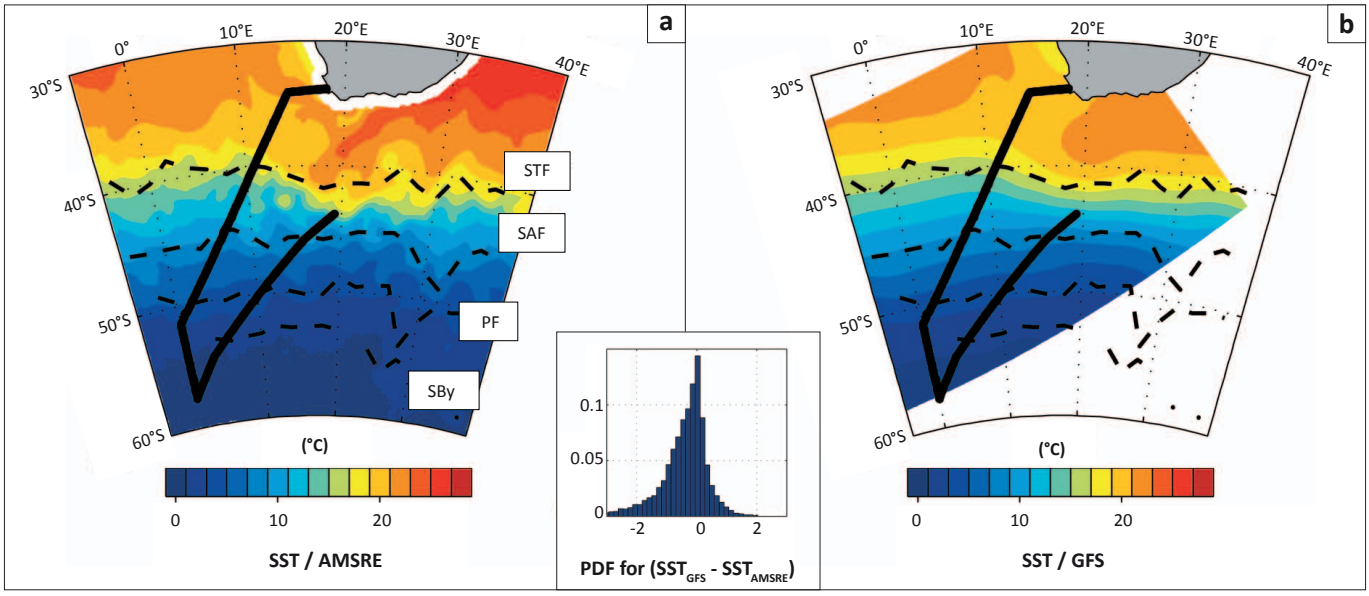

The fronts were located using Argo floats.[10]
The solid line indicates the ship's track and the dashed lines indicate the locations of the fronts: STF, Subtropical Front; SAF, Subantarctic Front; PF, Polar Front; SBy, Southern Boundary.

FIGURE 1: Average sea surface temperature (SST) for the period from 15 February to 20 March 2008 measured by (a) the Advanced Microwave Scanning Radiometer (AMSR-E) satellite and (b) the Global Forecast System (GFS) used for the Weather Research and Forecast simulations. The normalised density function of the difference between AMSR-E and GFS is inset.

The *in-situ* winds were compared to the twice daily, quarter-degree, gridded product derived from NASA's Quick Scatterometer high-resolution Sea Winds QuikSCAT[15] (Figures 2a and 2b). QuikSCAT data are produced by Remote Sensing Systems[16] (version 4) and sponsored by the NASA Ocean Vector Winds Science Team. QuikSCAT provides estimates of the 10-m-equivalent neutral wind speed, which is suitable for comparison with the observed wind converted to 10 m. Note that on 16 February and 23 February in the morning, the ship was located outside the satellite's observation range and QuikSCAT data were unavailable.

The sensible and latent heat fluxes deduced from the *in-situ* observations were computed using the Coupled Ocean Atmosphere Response Experiment (COARE) 'bulk flux' algorithm[17] and are presented in Figures 2c and 2d. The Woods Hole Oceanographic Institution's daily 1° x 1° Objectively Analyzed Air-sea Fluxes[18] (OAflux) data set was used as an air–sea regional data set. Here, '*in-situ* heat fluxes' refer to the heat fluxes calculated with COARE bulk formulae applied to ship measurements. Note that in this article positive heat fluxes are oriented upwards, that is, from the ocean to the atmosphere.

The model used to perform atmospheric forecasts was the Weather Research and Forecast model[19] (WRF) with non-hydrostatic Advance Research WRF (ARW) core and simple diffusion scheme. Two nested domains were defined (with resolutions of 37.5 km and 12.5 km) with 51 vertical levels. The inner one – the one used in this work – is nested with a two-way feedback method. The WRF physics of the two domains are set to Mellor-Yamada-Janjic for the planetary boundary layer scheme. The Noah 4-Layers land surface model was used together with the Monin–Obukhov–Janjic surface layer scheme, Grell–Devenyi Ensemble cumulus parameterisation and Rapid Radiative Transfer Model for long-wave and Goddard short-wave radiation schemes. The Ferrier microphysics scheme was turned on. During the cruise, the model performed a 24-h forecast with an hourly output step every day. The NCEP Global Forecast System (GFS) products were used for lateral boundary conditions and initial condition at 00:00 UTC.

The Advanced Microwave Scanning Radiometer (AMSR-E) satellite SST daily quarter-degree gridded product provided by Remote Sensing Systems was also used as a SST stand-alone product for comparing the SST provided by GFS (hereafter, GFS-SST) and used by the WRF model.

Wind analysis

QuikSCAT wind

During the entire cruise period, QuikSCAT and *in-situ* winds were highly correlated in time: $r = 0.97$ for wind speed and $r = 0.92$ for wind direction during Leg 1 and $r = 0.87$ for wind speed and $r = 0.77$ for wind direction during Leg 2. Wind speed and direction matched very well during the first week of the cruise, north of the STF (Figures 2a and 2b). However, south of the STF and across the ACC, QuikSCAT wind speeds were systematically lower than the *in-situ* observations. The average wind speed differences were 0.71 m/s before 28 February and 1.37 m/s after this date until the end of Leg 2 (20 March). A scatter plot of QuikSCAT versus *in-situ* winds (Figure 3a) shows that (1) 74% of the wind intensities retrieved by QuikSCAT were underestimated compared to *in-situ* measured wind and (2) these differences applied mainly to wind speeds larger than about 10 m/s.

The largest wind speed differences were observed on 01 March when the *in-situ* sustained wind speed reached more than 20 m/s for several hours (gale force wind). The two QuikSCAT wind speed estimates for this period were, respectively, 5.7 m/s and 5.3 m/s lower than those observed (Figure 3a).

Comparatively, QuikSCAT wind directions showed little differences when compared to *in-situ* measurements during the entire cruise (+12.7° in average, Figure 3b). For instance, QuikSCAT accurately captured the abrupt change in wind direction (of more than 90°) observed when the ship reached the Roaring Forties (westerly winds) on 25 February (40°S, 11.5°E). Also, under very high wind speed conditions, QuikSCAT wind directions were close to the observations. During the 01 March event, the satellite wind direction was only in the order of 1° lower than observed.

Under low wind speed conditions, QuikSCAT wind directions were consistent with the observations. On 19 February at midday and 20 February in the afternoon, the wind was particularly weak (< 3 m/s) and its direction variable (southerly on 19 February to north-north-easterly early on 20 February and then westerly in the evening). Wind direction differences were low during these two days (< 5°) except on 19 February afternoon, when the QuikSCAT wind direction difference reached -30°. Scatterometer wind direction is expected to be less accurate at wind speeds below 7 m/s when the remote signal is weak and easily confounded by noise.[20] However, the improved data retrieving methods of the data set used here are certainly a factor in this accuracy.

On 23 and 24 February, the ship crossed the STF and the wind speed increased accordingly. The front appeared as a strong SST gradient of -4 °C per 100 km observed at about midday (Figure 2e), and the increase in wind speed was in the order of 6 m/s. Although this observation suggests an interaction between the SST gradient and the wind, it is more accurately explained by a coincident synoptic weather pattern. A low pressure system located to the north of the ship and centred on the Cape Basin deepened on these days. The associated wind speed increase was accentuated by the eastward displacement of a high pressure system, which was located to the south along 43°S. For these reasons, the wind increased uniformly over a larger area and was not controlled by the front. Note that the influence of the front on the high pressure system's trajectory was not considered. Similarly, variations of wind speed and direction observed at the crossing of other fronts during the cruise were also as a consequence of coincident weather variability. Hence, the possible effects of frontal structures were masked by weather scale variability.

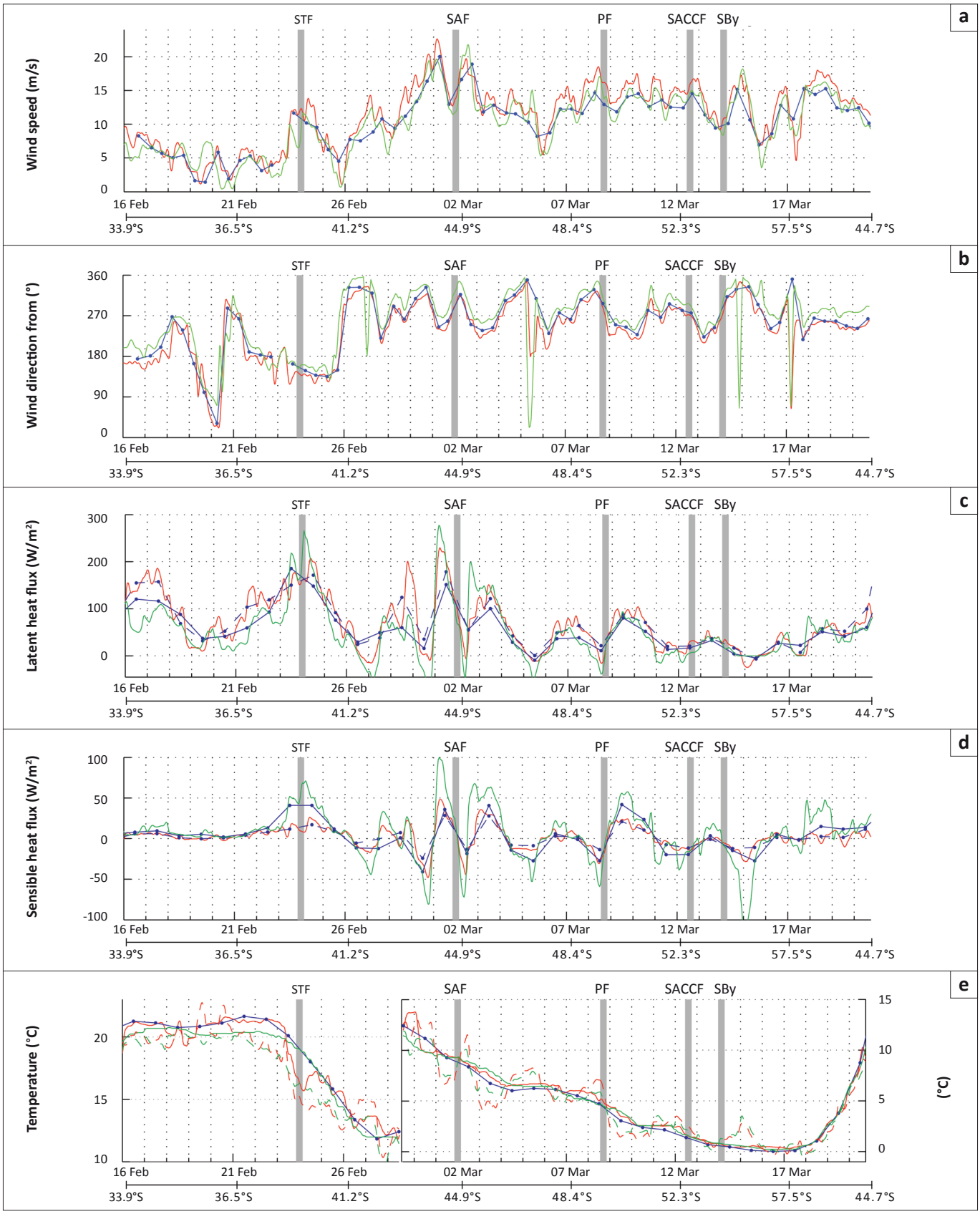

Vertical grey lines represent oceanic front locations: STF, Subtropical Front; SAF, Subantarctic Front; PF, Polar Front; SACCF, Southern Antarctic Circumpolar Current Front; SBy, Southern Boundary. The bottom horizontal scale gives latitudes and dates during the campaign. Along the time axis, each tick corresponds to 00:00 UTC.
Note: The vertical scale changes on 28 February at noon for Figure 2e only.

FIGURE 2: Time series of (a) wind speed, (b) wind direction – the direction from which the wind is blowing (meteorological convention), (c) latent heat flux and (d) sensible heat flux (positive values indicate upward fluxes). Red curves are the hourly *in-situ* observations, green curves are the hourly forecast, solid blue curves are the twice-daily QuikSCAT product for (a) and (b) and the daily OAflux product for (c) and (d). The time series in (e) shows the observed sea surface temperature (SST) in red, the SST of the Global Forecast System in green, the SST of the Advanced Microwave Scanning Radiometer in blue, the observed 2-m height air temperature by the dotted red curve, and the simulated 2-m height air temperature by the dotted green curve.

In one particular event on 05 March, QuikSCAT and *in-situ* winds (direction and intensity) had a similar temporal variability but their directions differed by about 50°. This discrepancy coincided with the passing of a low pressure system (data not shown). On this day, the observed wind abruptly reversed (northerly to southerly) and its intensity decreased by 6 m/s. The accompanying observed temperature increase (Figure 2e), as a result of the northerly wind, also illustrates this synoptic circulation effect. The rapid changes in wind direction and intensity (i.e. rapid wind rotations in intervals less than 12 h) were not well resolved at the correct time and location by the satellite as they occurred between two passes, resulting in an aliasing effect.

Model wind

The 10-m-height WRF and *in-situ* wind speeds were relatively well correlated in time (r = 0.79) over the entire cruise. However, this correlation was improved if data before 21 February was ignored (r = 0.90). The average difference between WRF and *in-situ* wind speeds was -1.32 m/s (Figure 3a), which is remarkable for 24-h weather forecasts. The WRF wind directions, on the other hand, were systematically biased north by 10° to 30° (Figure 3b), when compared to *in-situ* data. Contrasting with the overall performance of the model, the modelled wind speeds were significantly higher than those observed on two occasions. The first one, around 21 February, occurred when the ship was located to the north of the STF and the second one on 02 March, occurred as the ship encountered gale force winds. These two cases are discussed later.

Particularly inconsistent wind forecasts were apparent when the ship was located between the South African coast and the STF, in the so-called Cape Cauldron, where oceanic circulation is dominated by mesoscale dynamics.[3] Ocean features associated with these dynamics, such as eddies, fronts and filaments, induce local wind intensity distortions.[8,9] Consequently, not resolving these features in the forecast modelling system's surface boundary conditions may lead to inconsistent forecasted wind characteristics.[21,22] Figures 1a and 1b illustrate the differences between the AMSR-E SST and the GFS-SST used to force the WRF model. The GFS-SST product does not resolve oceanic mesoscale features, particularly over the Agulhas Retroflection but also close to the ACC fronts. This lack of accuracy, associated with the high-resolution model grid for sea surface conditions, induces unrealistic simulated winds.[22,23]

Another somewhat inconsistent forecast was produced during gale force winds starting on 29 February, which were associated with an abrupt wind acceleration on 01 March (near gale to strong gale winds – 986 hPa at 00:00 UTC) reaching 22.5 m/s at 06:00 UTC (Figure 4). This wind maximum was followed by an abrupt decrease in the wind intensity (to 13 m/s), followed by a second powerful wind outburst of ~20 m/s on 02 March. The storm was moving eastward, and was encountered as the ship was crossing the SAF (Figure 2a). During the first gale, the WRF model forecast underestimated the magnitude of the wind by

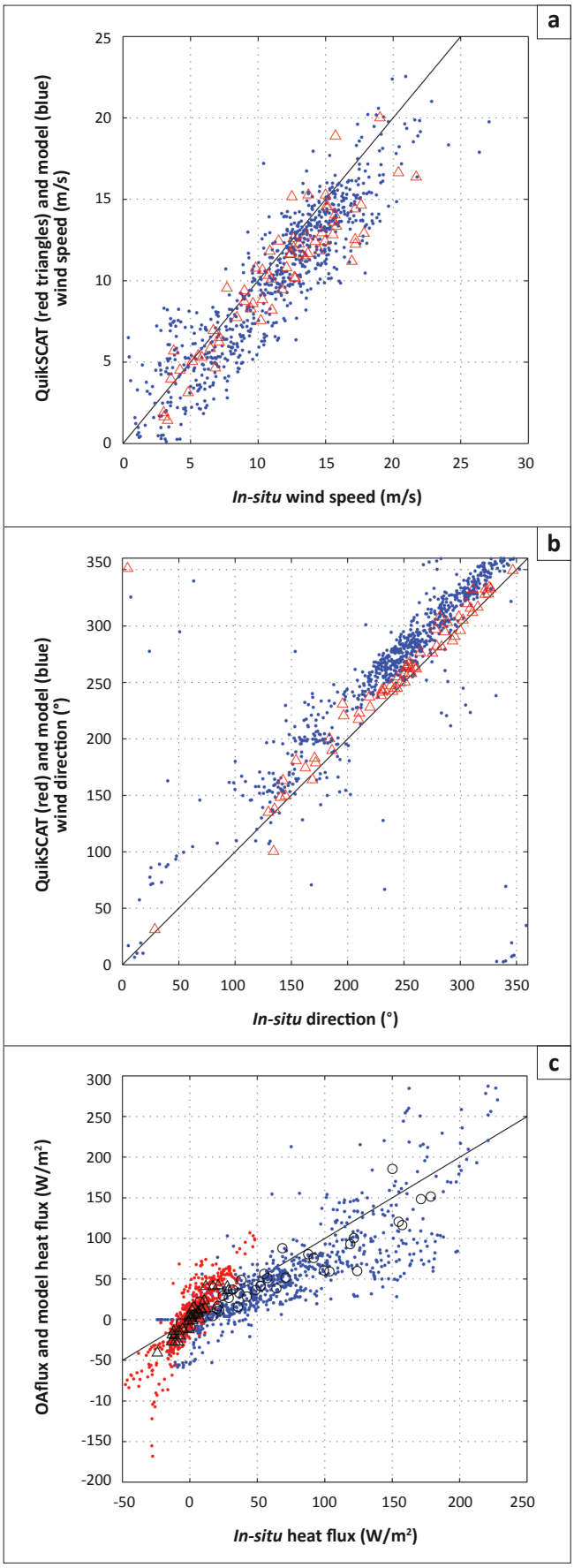

FIGURE 3: Scatter plots of (a) QuikSCAT (red triangles) and model (blue dots) data versus *in-situ* observations for wind intensity and (b) wind direction; and (c) OAflux latent (circles) and sensible (triangles) heat fluxes and model latent (blue dots) and sensible (red dots) heat fluxes. Positive values indicate upward heat fluxes.

2.8 m/s, whilst during the second gale it overestimated the wind by 2.1 m/s, relative to *in-situ* observations. Fortunately, the model successfully forecasted the time variability of the wind, as well as a significant increase in the wind speed, as needed for the ship's operations. This event is discussed further in the surface sensible and latent heat fluxes analysis.

Surface sensible and latent heat fluxes

OAflux fluxes

The daily OAflux latent heat fluxes (LHF) and sensible heat fluxes (SHF) were highly correlated with the daily averaged *in-situ* fluxes (r = 0.93 and r = 0.94, respectively, along Leg 1; and r = 0.99 and r = 0.87, respectively, along Leg 2). An underestimation occurred in 75% of the OAflux LHFs compared to *in-situ* LHFs (from -25 W/m^2 to -50 W/m^2; Figure 3c). The accuracy was better for LHF values lower than 100 W/m^2. The OAflux SHFs exhibited about as many underestimations as overestimations. However, the range of the differences between the *in-situ* and OAflux fluxes were similar for LHF and SHF.

OAflux LHF differences relative to the *in-situ* heat fluxes were large north of the STF (16–24 February), as well as in the Subantarctic zone (between STF and SAF; 27–29 February). These discrepancies are likely attributed to the relatively coarse 1° x 1° OAflux resolution, because strong LHF anomalies associated with mesoscale features are not well resolved. Indeed, warm eddies advected towards high latitudes of colder atmospheric conditions lose heat to the atmosphere mainly in the form of LHF. For instance, on the afternoon of 28 February, the ship's track intersected a warm anticyclonic eddy marked by a 1 °C increase in *in-situ* SST (Figure 2e) and a sharp increase in LHF (up to 200 W/m^2). This eddy was initially ejected from the Agulhas Retroflection about 9 months earlier, carrying warm Indian Ocean waters southward,[14] and producing an important heat flux towards the atmosphere (Figure 2c). The eddy, although clearly

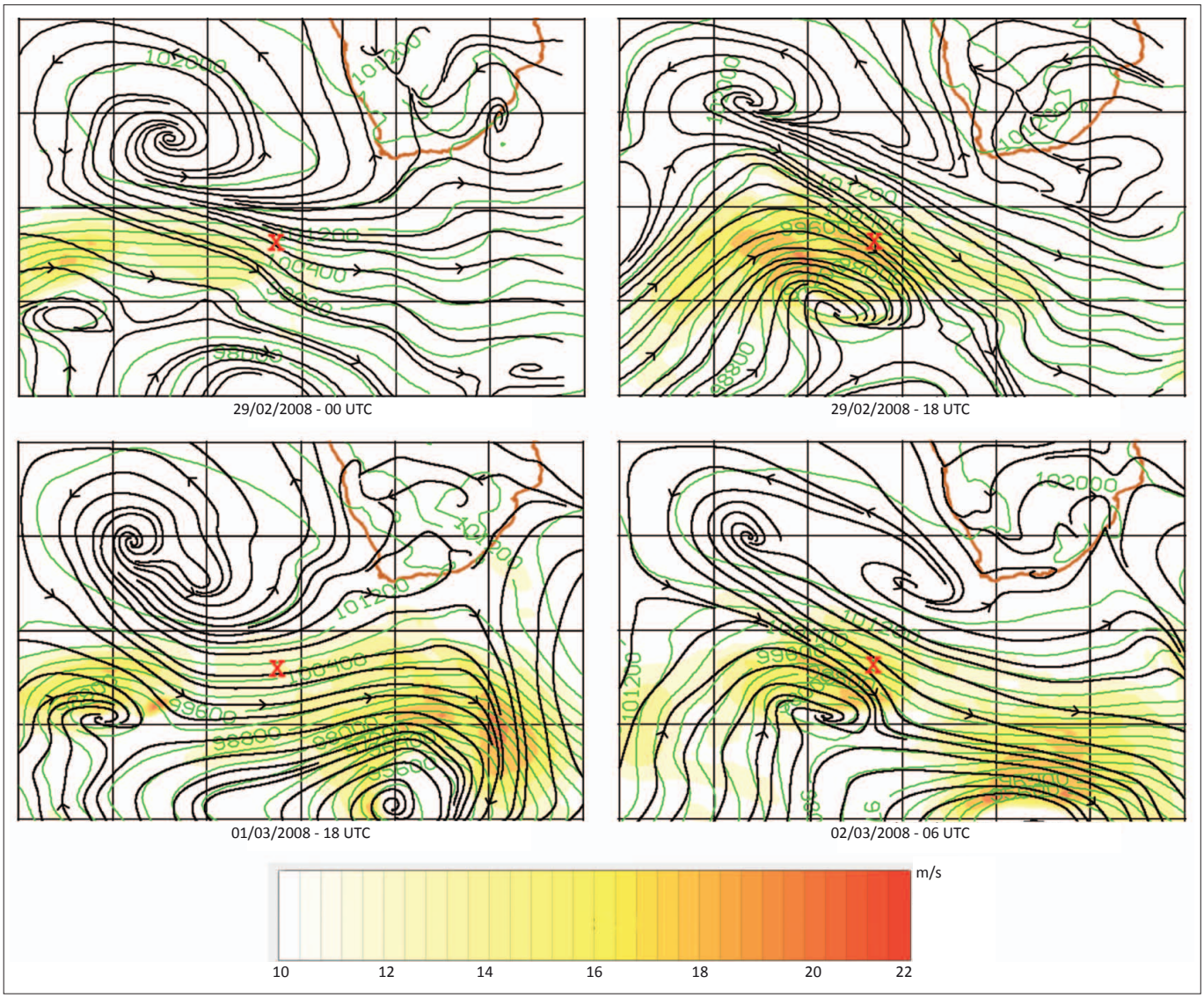

FIGURE 4: Synoptic weather conditions of the gale force winds that occurred from 29 February to 03 March 2008, provided by the European Centre for Medium-Range Weather Forecasts. Also shown are the 10-m wind streamlines (solid black lines); mean sea level pressure (in Pa, green contour) and wind intensity (colour filled contour). The red crosses represent the ship locations. The African coastline is shown in red. The first gale passing over the ship occurred from 29 February to 01 March. The second gale occurred on 02 March.

captured by the *in-situ* SST measurements, is absent from the OAflux SST. The resulting OAflux LHF underestimation was -70 W/m^2, relative to the *in-situ* observation.

A strong OAflux SHF overestimation (+30 W/m^2) was noticeable when the ship crossed the STF (23–24 February). The sharp meridional decrease in SST associated with the STF (and the anticyclonic warm eddy's southern edge), was not well resolved by the OAflux SST (or by the AMSR-ESST; Figures 1b and 2e). Because the SST was too high during these two days, the OAflux air–sea temperature gradient and SHF were overestimated relative to the *in-situ* data. This case is also discussed later.

Model fluxes

The hourly forecasted heat fluxes (0–24 h forecasts) were well correlated in time with the hourly *in-situ* heat fluxes (r = 0.78 for LHF). Differences between modelled and *in-situ* fluxes, similar to the ones found in OAflux, were characterised by underestimated LHF and SHF north of the STF, and underestimated LHF over the warm eddy that was crossed on 28 February. In contrast, modelled heat fluxes were overestimated when crossing the STF, during gale force winds (encountered from 29 February) and during condensation events at the ocean surface (negative LHF). Five interesting cases of differences in LHF and SHF are discussed further.

The modelled LHFs were generally underestimated when compared to the *in-situ* observations. The average difference over the cruise period was -23 W/m^2. However, the scatter plot of modelled versus *in-situ* LHF (Figure 3c) shows that differences were more widely spread for *in-situ* LHF larger than 100 W/m^2 and reached values up to -100 W/m^2. In contrast, for *in-situ* measurements larger than 200 W/m^2, modelled LHF were overestimated on average by +40 W/m^2 (Figures 1c and 3c).

The modelled SHFs were on average overestimated by a factor of about two (Figure 3c), that is, the model tended to underestimate negative SHFs and overestimate positive SHFs. The model generated large differences between *in-situ* observations and negative SHFs. For instance, on 15 March, a sharp peak in air temperature, likely caused by a warm air mass being advected by northerly winds, was associated with a large modelled SHF to the ocean, which was overestimated by -150 W/m^2 (negative fluxes are downwards) relative to *in-situ* observations.

North of the STF, LHF underestimation was particularly important. In this area, both GFS-SST (model boundary condition) and forecasted wind speed were significantly underestimated by up to 1.2 °C (Figure 2e) and 1 m/s, respectively, as discussed earlier.

The case of the eddy crossing on 28 February illustrates the lack of accuracy of the simulated fluxes because the GFS-SST used to force the model did not contain the observed eddy (Figure 2e). Note that the modelled air temperature dropped by about 2.5 °C over the eddy, producing an increase in SHF of 30 W/m^2 and in LHF of 50 W/m^2 out of the ocean. However, the link between this temperature drop and the presence of the eddy is unclear.

At the STF (23 February 12:00 UTC to 25 February), the SST used by the model (GFS-SST) was up to 3 °C higher than the observed SST. Because the air was colder than the ocean, the modelled sea–air temperature gradient was overestimated. Consequently, the ocean heat loss to the atmosphere (SHF and LHF) was overestimated, relative to *in-situ* data (Figure 2e), even though the model air surface temperature was also higher than observed (Figures 2c, 2d and 2e). The STF in the surface model condition was thus too smooth. The overestimation of SHF and LHF over the STF, also seen in the OAflux comparison, was thus likely because of the lack of mesoscale structure in the GFS-SST.

The differences between the *in-situ* and modelled surface fluxes in the case of the gale force winds (from 29 February to 02 March; Figure 4), are also important to note. On 29 February, the air temperature in the model was 1.5 °C to 2 °C lower than that observed, whilst the differences between the *in-situ* and modelled SST became insignificant. These discrepancies induced an important difference in the sea–air temperature gradient, which resulted in underestimated LHF and SHF, relative to the *in-situ* observations (up to +50 W/m^2). Similarly, on 01 March, the forecasted air temperature was higher than that observed and both LHF and SHF were overestimated relative to *in-situ* data. The same phenomena occurred on 02 March during the second gale. These inconsistent forecasts were as a result of two factors, (1) the forecasted arrival of the storm, and associated south-eastward warm air flux, was delayed and (2) the storm's trajectory toward the east was inaccurately modelled.

Negative values of LHF, corresponding to events of condensation at the ocean surface by which the ocean gains heat, were underestimated by up to -50 W/m^2 relative to observations (e.g. on 29 February in the afternoon; Figure 1c). Such an event occurred six times during the cruise. Note that on 15 March, south of the SBy, the *in-situ* LHF reached -25 W/m^2, whereas the modelled LHF stayed close to 0 W/m^2.

On 05 March 06:00 UTC and 16 March 18:00 UTC, low-pressure system trajectories were forecasted in an overly north-eastward direction. These incorrect trajectories were responsible for the large errors in wind direction and intensity, which in turn induced important differences between observed and forecasted heat fluxes.

Discussion and conclusion

During the BONUS-GoodHope cruise, both QuikSCAT and WRF wind speeds were lower than those observed from the ship. South of the STF, the averaged QuikSCAT (WRF) differences relative to *in-situ* data were -1.37 m/s (-1.32 m/s)

for wind speed, and +12.7° (+10° to +30°) for wind direction. Because the differences found between QuikSCAT and *in-situ* data are within the range of acceptable errors of the QuikSCAT specifications (which are ±2 m/s and ±20° for wind speeds between 3 m/s and 20 m/s), the satellite product can be used to assess the WRF wind field over the domain of the model.

The wind speed differences between WRF and QuikSCAT, temporally averaged over the cruise period (Figure 5a), were low over most of the model's domain, and never exceeded 0.75 m/s, which is below QuikSCAT uncertainties (± 2 m/s), indicating that the model performed well when compared to QuikSCAT. However, the sign of this difference reversed about 2° south of the STF; the modelled 10-m winds were underestimated north of the STF and overestimated south of the STF, relative to QuikSCAT winds. The analysis of the wind component differences revealed that this remarkable observation was associated with the zonal component (Figure 5b), rather than the meridional component differences (not shown). As the region north of the STF is characterised by a strong mesoscale variability, the differences revealed in the simulated wind field are likely to be related to the SST mesoscale variability influence on the wind.[9,24] The model is actually able to reproduce a signal associated with the presence, or lack thereof, of mesoscale (from 100 km to 500 km) oceanic features. The spatial reliability of the model output is indeed considered close to 37.5 km (3 x 12.5 km) rather than the native resolution of 12.5 km (the spatial reliability is usually based on a combination of the eight points surrounding a grid point). Mesoscale structures seen on the AMSR-E SST field (Figure 1a) were not resolved by the GFS-SST (Figure 1b). The AMSR-E SST exhibited important mesoscale activity (meanders and eddies) at the Benguela upwelling system and Agulhas Retroflection area, extending up to 2° of latitude south of the STF. The correspondence of this structure to the wind zonal component of Figure 5b suggests that the smoothed GFS-SST field had an impact on the modelled wind field. The impact of a high-resolution SST variability on wind simulations has been underlined[22] in previous studies, particularly for initial conditions in simulations.[25] Additionally, it is important to note that (1) the other oceanic fronts crossed during the cruise did not appear to cause a perturbation in the wind forecast and (2)

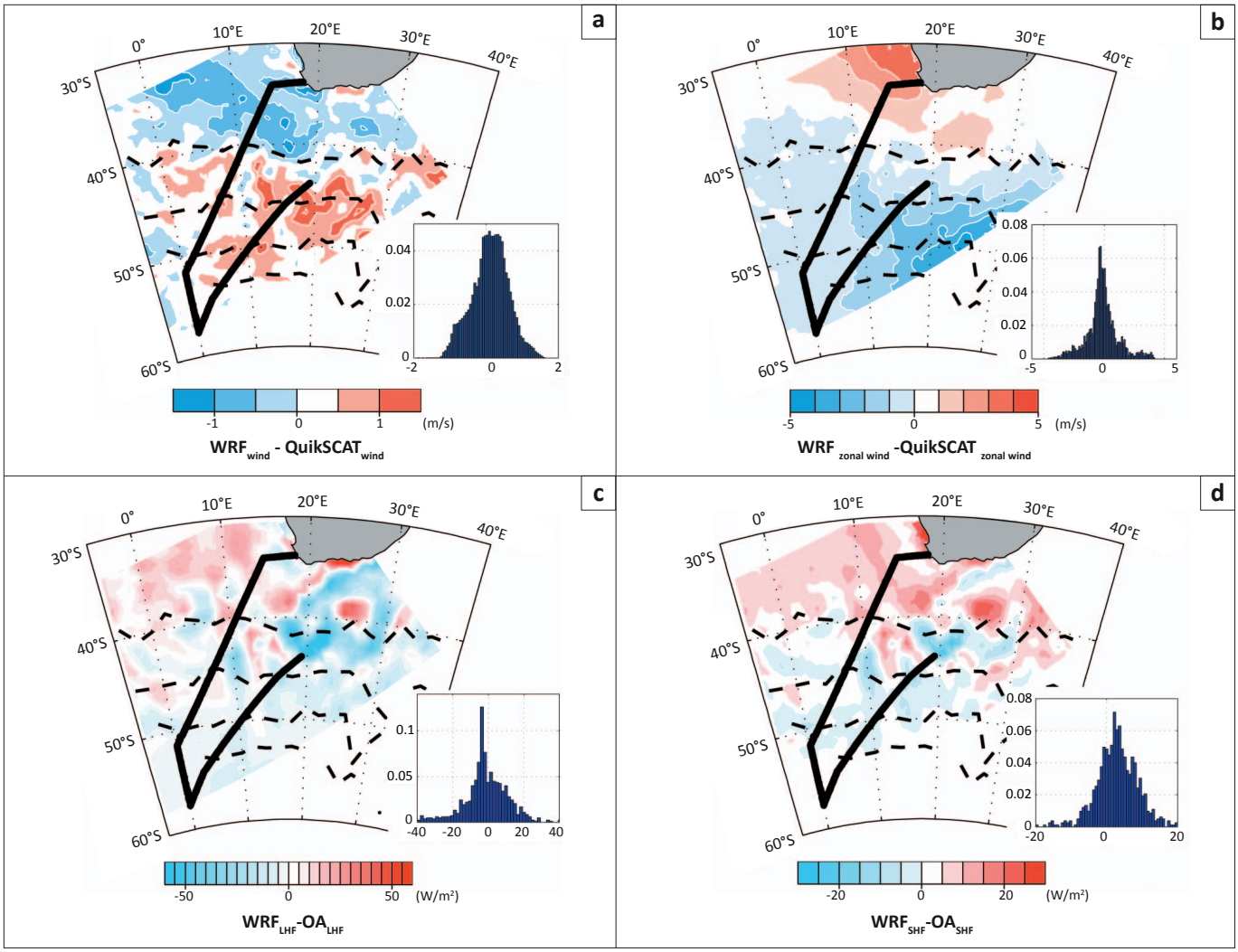

FIGURE 5: The average (a) wind speed and (b) zonal wind component differences between the daily simulated (WRF) and QuikSCAT winds; and the (c) latent (LHF) and (d) sensible heat flux (SHF) differences between daily simulated and OAflux fluxes from 15 February to 20 March 2008. Normalised density functions of the differences are inset.

uncertainties regarding the intensities and trajectories of atmospheric low-pressure systems seem to produce biases in the wind direction forecast accuracy.

The daily OAflux heat fluxes corresponded well to *in-situ* observations. Indeed, the ship track crossed several oceanic and atmospheric abrupt fronts and both OAflux LHF and SHF followed very well the spatial and time *in-situ* variability, except across the STF. The OAflux data set is thus relevant for comparison with the heat fluxes produced by WRF over the model domain (Figures 5c and 5d). Most of the differences between OAflux and model outputs were below 20 W/m^2 for LHF and 5 W/m^2 for SHF, with the exception of the warm anticyclonic eddy crossed on 29 February. Similar to those of the wind field, larger differences were located over areas of intensive mesoscale dynamics (the Agulhas Retroflection, Cape Cauldron and Benguela regions), unresolved by the GFS-SST (Figures 1a and 1b) which is the only ocean–surface boundary condition of the WRF model. Consequently, the spatial resolution was too coarse to resolve realistic spatial variability of ocean–atmosphere energy transfer.

It is remarkable that the spatial pattern of LHF and SHF differences resemble the high-resolution SST pattern (Figure 1a and Figure 5c) over the Agulhas Retroflection. The relative bias between the model and OAflux data sets (i.e. the difference between the model and OAflux data divided by the model data; not shown) reveals that the forecasted SHF had a higher relative bias than did LHF over the Agulhas Retroflection, Cape Cauldron and Benguela regions. High relative bias in SHF indicates that the simulated air–sea temperature gradient is inaccurate. Although the GFS-SST bias underlined above partly explains this inaccuracy, biases in the modelled 2-m-height air temperature also play a role.

Indeed, the modelled 2-m-height air temperature presented important biases when compared to *in-situ* observations (Figure 2e). The modelled 2-m-height air temperature inaccuracies were directly related to GFS-SST inaccuracy for some cases. However, in other cases, they were as a result of inaccurate air mass fluxes, associated with the inaccurate displacement of meteorological synoptic weather features in the model outputs.

This work also shows that the daily QuikSCAT data and hourly WRF wind forecast were reasonably accurate in terms of temporal and spatial variability with a systematic underestimation (of 1 m/s to 2 m/s) south of the STF during the summer of 2008. The WRF forecast also underestimated the extreme event of 01 March but clearly indicated a wind enhancement (exceeding the range of safe operation for the oceanographic instruments) with the deepening of a low pressure. The on-board scientific team was thus able to anticipate the storm based on the WRF forecast only. Note that marine weather forecasts provided by weather services were unavailable on the ship from 29 February to 04 March. The WRF model, which was successfully used in operational mode, was also easy and fast to set up.

Finally, this work also underlines the strong sensitivity of the simulated LHFs and SHFs to the model's prescribed SST. The simulated wind is sensitive to important SST gradients (associated to mesoscale oceanic features) which are often not well represented in the surface fields used by WRF for initial and sea-surface boundary conditions. For instance, the smoothed SST gradient of the STF induced an overestimation of the LHFs and SHFs. However, the otherwise relative accuracy of the forecasted heat fluxes encourages the use of regional models to study annual to interannual ocean–atmosphere exchange processes. The LHF was indeed the most efficient process transferring heat from the ocean to the atmosphere. The mean *in-situ* Bowen ratio along the ship track (0.041) indicates that a major part of the energy available at the ocean surface was passed to the atmosphere through evaporative processes (the evaporation fraction was 0.96).

Modelling and forecast improvements obtained with the use of high-resolution MODIS SST have already been demonstrated.[22] However, the use of a high-resolution satellite product is useful only for short-term weather forecasts (< 12 h) because observations are able to provide the initial conditions only. For longer weather forecasts, the use of a high-resolution oceanic forecast product should be preferable. Alternatively, the use of a diurnal SST prognostic scheme[26] could improve forecasts.

Acknowledgements

We are thankful to the crew of the R/V *Marion Dufresne*-IPEV. The IPY/BONUS-GoodHope project is supported by the Institut National des Sciences de l'Univers, the CNRS, the IFREMER and the Agence Nationale de la Recherche. We are also thankful to Prof. Peter J. Minnet (RSMAS) for the sharing of instruments and to Dr Erica Key for observation calibrations and *in-situ* data treatments. Finally, all the operational forecasts were performed with the IFREMER-CAPARMOR HPC facilities and its staff support.

Competing interests

We declare that we have no financial or personal relationships which may have inappropriately influenced us in writing this article.

Authors' contributions

C.M. was the project leader and performed some of the *in-situ* observations, the simulations and the analysis, and wrote the manuscript. V.F. participated in the analysis and contributed to the manuscript.

References

1. Bryden HL, Beal LM, Duncan LM. Structure and transport of the Agulhas Current and its temporal variability.J Oceanogr. 2005;61:479–492. http://dx.doi.org/10.1007/s10872-005-0057-8
2. Lutjeharms JRE, Van Ballegooyen RC. The retroflexion of the Agulhas Current. J Phys Ocean. 1988;18:1570–1583.
3. Boebel O, Lutjeharms J, Schmid C, Zenke W, Rossby T, Barron C. The Cape Cauldron: A regime of turbulent inter-ocean exchange. Deep Sea Research II. 2003;50:57–86. http://dx.doi.org/10.1016/S0967-0645(02)00379-X

4. Lutjeharms JRE. The Agulhas Current. Heidelberg: Springer-Verlag; 2006.
5. Jury MR, Walker N. Marine boundary layer modification across the edge of the Agulhas Current. J Geophys. Res1988;93:647–654. http://dx.doi.org/10.1029/JC093iC01p00647
6. Lee-Thorp AM, Rouault M, Lutjeharms JRE. Moisture uptake in the boundary layer above the Agulhas Current: A case study. J Geophys Res. 1999;104:1423–1430. http://dx.doi.org/10.1029/98JC02375
7. Rouault M, Lutjeharms JRE. Air–sea exchanges over an Agulhas eddy at the subtropical convergence. Global Atmos–Ocean Syst. 2000;7:125–150.
8. O'Neill L, Chelton D, Esbensen S, Wentz F. High-resolution satellite measurements of the atmospheric boundary layer response to SST variations along the Agulhas Return Current. J Climate. 2005;18:2706–2723. http://dx.doi.org/10.1175/JCLI3415.1
9. Small RJ, DeSzoeke SP, Xie SP, et al. Air–sea interaction over ocean fronts and eddies. Dyn Atmos Oceans. 2008;45:274–319. http://dx.doi.org/10.1016/j.dynatmoce.2008.01.001
10. Faure V, Arhan M, Speich S, Gladyshev S. Heat budget of the surface mixed layer south of Africa. Ocean Dynamics. 2011;61(10):1441–1458. http://dx.doi.org/10.1007/s10236-011-0444-1
11. Orsi AH, Whitworth III T, Nowlin WD. On the meridional extent and fronts of the Antarctic Circumpolar Current. Deep Sea Research I. 1995;42:641–673. http://dx.doi.org/10.1016/0967-0637(95)00021-W
12. Belkin IM, Gordon AL. Southern Ocean fronts from the Greenwich meridian to Tasmania. J Geophys Res. 1996;101:3675–3696. http://dx.doi.org/10.1029/95JC02750
13. Dencausse G, Arhan M, Speich S. Spatio-temporal characteristics of the Agulhas Current Retroflection. Deep Sea Research I. 2010;57(11):1392–1405. http://dx.doi.org/10.1016/j.dsr.2010.07.004
14. Arhan M, Speich S, Messager C, Dencausse G, Fine R, Boyé M. Anticyclonic and cyclonic eddies of subtropical origin in the subantarctic zone south of Africa. J Geo Res. 2011;116:C11004. http://dx.doi.org/10.1029/2011JC007140
15. Ricciardulli L, Wentz F. Reprocessed QuikSCAT (V04) wind vectors with Ku-2011 geophysical model function. Remote Sensing Systems Technical Report 043011. Santa Rosa, CA: Remote Sensing Systems; 2011.
16. Remote Sensing Systems. Version-4 QuikSCAT Ocean Surface Wind Vectors [homepage on the Internet]. c2011 [updated 2011 June 29; cited 2011 Dec 12]. Available from: http:// www.remss.com
17. Fairall CW, Bradley EF, Hare JE, Grachev AA, Edson JB. Bulk parameterization on air–sea fluxes: Updates and verification for the COARE algorithm. J Climate. 2003;16:571–591. http://dx.doi.org/10.1175/1520-0442(2003)016<0571:BPOASF>2.0.CO;2
18. Woods Hole Oceanographic Institution. Objectively Analyzed Air–sea Fluxes (OAflux) for the global oceans, a project funded by the NOAA Climate Observations and Monitoring (COM) program [homepage on the Internet]. c2008 [updated 2011 Nov 03; cited 2011 Dec 12]. Available from: http://oaflux.whoi.edu/
19. Skamarock WC, Klemp JB, Dudhia J, et al. A description of the Advanced Research WRF Version 3. NCAR Technical Note 2008 NCAR/TN–475+STR [document on the Internet]. c2008 [updated 2008 June 01; cited 2011 Dec 12]. Available from: http://www.mmm.ucar.edu/wrf/users/docs/arw_v3.pdf
20. Yueh SH, Wilson WJ, Dinardo SJ, Li FK. Polarimetric microwave brightness signatures of ocean wind directions. IEEE Trans Geosci Remote Sensing. 1999;37(2):949–959. http://dx.doi.org/10.1109/36.752213
21. LaCasse KM, Splitt ME, Lazarus SM, Lapenta WM. The impact of high resolution sea surface temperatures on short-term model simulations of the nocturnal Florida marine boundary layer. Mon Wea Rev. 2008;136(4):1349–1372. http://dx.doi.org/10.1175/2007MWR2167.1
22. Song Q, Chelton DB, Esbensen SK, Thum N, O'Neill LW. Coupling between sea surface temperature and low-level winds in mesoscale numerical models. J Climate. 2009;22:146–164. http://dx.doi.org/10.1175/2008JCLI2488.1
23. O'Neill L, Esbensen S, Thum N, Samelson R, Chelton D. Dynamical analysis of the boundary layer and surface wind responses to mesoscale SST perturbations. J Climate. 2010;23:559–581. http://dx.doi.org/10.1175/2009JCLI2662.1
24. Chelton DB, Schlax MG, Samelson RM. Summertime coupling between sea surface temperature and wind stress in the California Current System. J Phys Oceano. 2007;37(3):495–517. http://dx.doi.org/10.1175/JPO3025.1
25. Case JL, Crosson WL, Kumar SV, Lapenta WM, Peters-Lidard CD. Impacts of high-resolution land surface initialization on regional sensible weather forecasts from the WRF model. J Hydrometeor. 2008;9:1249–1266. http://dx.doi.org/10.1175/2008JHM990.1
26. Zeng X, Beljaars A. A prognostic scheme of sea surface skin temperature for modeling and data assimilation. Geophys Res Lett. 2005;32:L14605. http://dx.doi.org/10.1029/2005GL023030